mathematics

MDPI

Article

Active Disturbance Rejection Strategy for Distance and Formation Angle Decentralized Control in Differential-Drive Mobile Robots

Mario Ramírez-Neria [1], Jaime González-Sierra [2], Alberto Luviano-Juárez [3], Norma Lozada-Castillo [3] and Rafal Madonski [4,*]

[1] InIAT Institute of Applied Research and Technology, Universidad Iberoamericana Ciudad de México, Prolongación Paseo de la Reforma 880, Colonia Lomas de Santa Fé, Ciudad de México 01219, Mexico
[2] Unidad Profesional Interdisciplinaria de Ingeniería Campus Hidalgo, Instituto Politécnico Nacional, Carretera Pachuca-Actopan Kilómetro 1+500 Ciudad del Conocimiento y la Cultura Educación, San Agustín Tlaxiaca 42162, Mexico
[3] Unidad Profesional Interdisciplinaria en Ingeniería y Tecnologías Avanzadas, Instituto Politécnico Nacional, Av. IPN 2580, Col. Barrio La Laguna Ticomán, Ciudad de México 07340, Mexico
[4] Energy and Electricity Research Center, Jinan University, Zhuhai 519070, China
* Correspondence: rafal.madonski@jnu.edu.cn

Abstract: The important practical problem of robust synchronization in distance and orientation for a class of differential-drive mobile robots is tackled in this work as an active disturbance rejection control (ADRC) problem. To solve it, a kinematic model of the governed system is first developed based on the distance and formation angle between the agents. Then, a special high-order extended state observer is designed to collectively estimate the perturbations (formed by longitudinal and lateral slipping parameters) that affect the kinematic model. Finally, a custom error-based ADRC approach is designed and applied assuming that the distance and orientation between the agents are the only available measurements. The proposed control strategy does not need time-derivatives of the reference trajectory, which increases the practical appeal of the proposed solution. The experimental results, obtained in laboratory conditions with a set of differential-drive mobile robots operating in a leader–follower configuration, show the effectiveness of the proposed governing scheme in terms of trajectory tracking and disturbance rejection.

Keywords: active disturbance rejection control (ADRC); differential-drive mobile robots; multi-robot control; formation control; extended state observer (ESO); robust control

MSC: 70E60

Citation: Ramírez-Neria, M.; González-Sierra, J.; Luviano-Juárez, A.; Lozada-Castillo, N.; Madonski, R.; Active Disturbance Rejection Strategy for Distance and Formation Angle Decentralized Control in Differential-Drive Mobile Robots. *Mathematics* **2022**, *10*, 3865. https://doi.org/10.3390/math10203865

Academic Editors: Paolo Mercorelli, Oleg Sergiyenko and Oleksandr Tsymbal

Received: 28 September 2022
Accepted: 17 October 2022
Published: 18 October 2022

1. Introduction

1.1. Motivation

The coordination of multiple mobile robots has been widely studied in recent years by both academic researchers and industry practitioners, as shown in surveys [1,2]. The progress made in this field allowed the development of important real-world applications, including surveillance, home services, and logistics [3]. The multiple mobile robots coordination problem extends the classical control, related to point convergence and trajectory tracking of a single mobile robot, to the case of collective behaviors, like the convergence to formation patterns, formation tracking, dispersion, containment, and inter-robot collision avoidance, among others.

The most basic scheme of multi-robot formation tracking is the case of two robots, where a leader agent follows a desired trajectory while the follower agents must keep a desired position and orientation with respect to the leader [4–6]. In a decentralized scheme, the multi-robot control methodology depends on the local measurements of distance and direction or absolute orientation [7]. From the vast area of decentralized multi-robot control, our work focuses on the challenge of robust formation control for differential-drive mobile robots or first order agents.

1.2. Related Works

To address the issue of decentralized formation control, different solutions have been proposed so far. For instance, a decentralized feedback law was presented in the pioneer work [8]. A control law that only depends on the distance and/or bearing angle measurements was proposed in [9–12]. In [13], a control law was developed using the gradient vector field based approach. An adaptive dynamic feedback with an immersion and invariance estimation-based second order sliding mode control was designed in [14]. A control strategy that combines kinematic controller based on Lyapunov theory with a dynamic controller based on sliding mode was proposed in [15]. It is worth pointing out that in [9,10], even though the control strategy is designed to be robust, there are still oscillations in the distances between the agents. Moreover, if there is noise in the measurement, the distances between agents start to oscillate. In [11], the main drawback is that the leader stays static. On the other hand, in [9,10,12,14,15] it is assumed that the leader's velocity is constant or it moves with a low velocity. Furthermore, none of the cited references consider perturbations that affect the kinematic model, and most of them only present simulation results. On the other hand, the existing physical systems are often affected by various types of uncertainties, like information delays, external disturbances, non-modeled dynamics, low energy storage in the agents, and/or possible unexpected frictions. This motivates to look for actual robust control schemes, that would allow the use of models with only partial system knowledge and could handle scenarios in which the robots are subject to uncertainties.

Another problem that arises when performing formation control in a multi-agent system is related to communication. In the first instance, there is a central computer where the control inputs are calculated and sent, via radio frequency, Bluetooth, or WiFi, to each of the agents. It is well known that wireless communication systems often have time delays and loss of information [16]. However, in recent years, different communication protocols have been developed [17,18] and have presented improvements in sending/receiving data as well as minimal information loss [19,20].

To address the above limitations of current control designs, an active disturbance rejection control (ADRC, [21,22]) scheme can be applied to solve the robust formation control for differential-drive mobile robots. The relative tuning simplicity of ADRC, together with its desirable features for practical applications [23,24], have made it an attractive alternative to standard controllers (e.g., PID-type) for tackling real-world control problems [25]. The ADRC, as a control philosophy, is based on the simplification of the control system, such that it can be represented as the control of a disturbed chain of integrators, in which the *total disturbance* aggregates all the internal and external disturbing effects, which are estimated by an extended state observer (ESO; see [26–28] for a comprehensive review of the topic) and further canceled out in the control law.

In light of the above advantages, there has been a considerable effort in the last few years to utilize ADRC in mobile robotics. The concept of ADRC has been previously considered for the trajectory tracking control of differentially flat mobile robots, particularly omnidirectional, which have the advantage of being of holonomic nature in contrast with the differential ones. For example, ADRC with high-order observer has been proposed in [29]. A combination of ADRC, model predictive control, and friction compensation was introduced in [30]. In [31], an ADRC-based trajectory tracking control was designed for an omnidirectional mobile manipulator operating in the presence of parameter uncertainties and external disturbances. The combination of ADRC and flatness is specially useful for mobile robots since flatness trivializes the trajectory planning task [32], allowing to ensure a robust trajectory tracking behavior. However, even when ADRC-based schemes are robust with minimal information of the system to control, the flatness-based ADRC requires the knowledge of the high order time derivatives of the reference trajectory, which, for the case of leader–follower schemes, is not regularly available.

1.3. Contribution

In this work, a special version of ADRC is proposed for differential-drive mobile robots. It relies on an error-based modification of ADRC, introduced in [33] (later generalized and proved in [24]). The main idea behind it is to make the implementation of ADRC resemble that of those currently used industrial solutions (like PID), hence making it easier to implement in real applications or to swiftly replace the existing control algorithm. This error-based adaptation already found itself useful in various control scenarios, like robust tracking in an under-actuated mass-spring system [34], altitude/attitude control of a quadrotor UAV [35], and motion control in robotic manipulators [36,37].

To summarize, the contribution of this paper is the proposition of a robust control strategy to solve the formation control problem based on the distance and formation angle between differential-drive mobile robots. The main distinctive features of the proposed control solution are as follows:

- It utilizes the robust ADRC scheme (with a custom error-based high-order ESO) that allows the follower agent to keep a desired distance and formation angle with respect to its own leader in spite the external disturbances, i.e., linear and lateral slipping parameters as well as unknown leader dynamics and velocities.
- It only depends on the distance and formation angle measurements.
- It is developed using solely a kinematic model based on the distance and the formation angle between a pair of robots, taking into account the front point of the differential-drive mobile robots.

To the authors' best knowledge, such an approach has not been yet presented in the available literature.

2. Leader–Follower Problem

2.1. Considered Class of Systems

Let $N = \{R_1, \ldots, R_n\}$ be a set composed of n differential-drive mobile robots moving in the horizontal plane, as depicted in Figure 1.

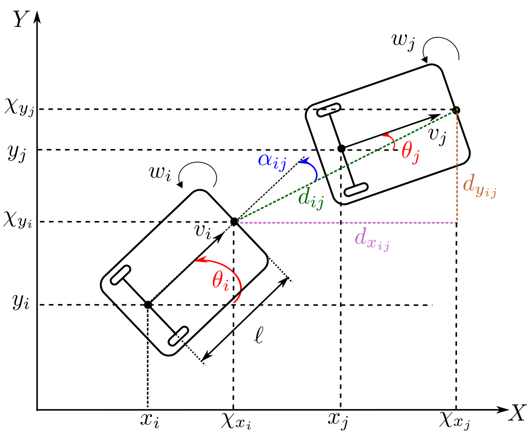

Figure 1. Schematic diagram of two differential-drive wheeled mobile robots in the leader–follower configuration.

The set of equations that describe the perturbed kinematic motion of the differential-drive mobile robots is defined as

$$\dot{\boldsymbol{\xi}}_i = G(\theta_i)\mathbf{u}_i + \boldsymbol{\varphi}_i(t), \quad i = 1, \ldots, n, \tag{1}$$

where R_n is the leader agent while $R_1, \ldots, R_{n-1}$ are the followers and $G(\theta_i)$ is the system matrix, defined by

$$G(\theta_i) = \begin{bmatrix} \cos\theta_i & 0 \\ \sin\theta_i & 0 \\ 0 & 1 \end{bmatrix},$$

where $\boldsymbol{\xi}_i = \begin{bmatrix} x_i & y_i & \theta_i \end{bmatrix}^\top \in \mathbb{R}^3$ is the state vector with $x_i \in \mathbb{R}$, $y_i \in \mathbb{R}$ as the position in the plane of the i-th agent, $\theta_i \in \mathbb{R}$ is the orientation with respect to the horizontal axis, $\mathbf{u}_i = \begin{bmatrix} v_i & \omega_i \end{bmatrix}^\top$ is the control input vector, where $v_i \in \mathbb{R}$ represents the longitudinal velocity and $\omega_i \in \mathbb{R}$ is the angular velocity; $\boldsymbol{\varphi}_i = \begin{bmatrix} \varphi_{x_i} & \varphi_{y_i} & 0 \end{bmatrix}^\top$ is the disturbance vector, which corresponds to the lateral and longitudinal slipping parameters of the wheels (this class of disturbance does not affect the orientation angle [38,39]). It is well known that when one tries to control the coordinates x_i, y_i, from (1), the system cannot be stabilized with a continuous and time-invariant control law due to singularities in the controller [40]. In order to avoid such singularities, it is proposed to study the kinematics of a point $\boldsymbol{\chi}_i$, located at a distance l from the midpoint of the wheels' axle of the mobile robot, defined as

$$\boldsymbol{\chi}_i = \begin{bmatrix} \chi_{x_i} \\ \chi_{y_i} \end{bmatrix} = \begin{bmatrix} x_i + l\cos\theta_i \\ y_i + l\sin\theta_i \end{bmatrix}.$$

The kinematics of the point $\boldsymbol{\chi}_i$ is computed as

$$\dot{\boldsymbol{\chi}}_i = A_i(\theta_i, l)\mathbf{u}_i + \boldsymbol{\varphi}_i, \tag{2}$$

with $A_i = \begin{bmatrix} \cos\theta_i & -l\sin\theta_i \\ \sin\theta_i & l\cos\theta_i \end{bmatrix}$ being the decoupling matrix, which is non-singular since $\det(A_i) = l \neq 0$.

Assumption 1. *The perturbations $\boldsymbol{\varphi}_i$ are smooth and bounded, where $\sup_t|\varphi_{x_i}| \leq K_x$ and $\sup_t|\varphi_{y_i}| \leq K_y$, with K_x and K_y being sufficiently large, positive, real numbers.*

Remark 1. *The studied class of systems is of passive nature and with bounds of inertia [41]; hence, Assumption 1 is practically justified and can be found in various robotic systems [42].*

Remark 2. *The capacity of the system to reject perturbations and disturbances is closely related to the fact that the flatness property (which involves the controllability) is preserved, which implies that the rolling lacks slipping conditions [43] (for instance, when there is a wheel skidding due to slippery floor). This condition represents the relation between the angular movement of the wheels' axes and the generated tangential movement of the wheels in contrast with slipping conditions due to external disturbances that are to be compensated by the control scheme. Thus, the controllability condition in each wheel is assumed to be satisfied in this work.*

2.2. Problem Statement

The considered problem can be divided into two subproblems: modeling and control. For the first one, a kinematic model of a pair of differential-drive mobile robots, based on distance and formation angle between agents, has to be developed by taking into account the front point $\boldsymbol{\chi}_i$, i.e.,

$$\dot{\boldsymbol{\eta}}_{ij} = \begin{bmatrix} \dot{d}_{ij} & \dot{\alpha}_{ij} \end{bmatrix}^\top = f(\boldsymbol{\eta}_{ij}, \theta_i, \theta_j, \mathbf{u}_i, \mathbf{u}_j),$$

where $d_{ij} \in \mathbb{R}^+$ is the Euclidean distance measured from the front point of R_i to the front point of R_j, with $\mathbb{R}^+$ as the set of all positive real numbers, $d_{x_{ij}}$ and $d_{y_{ij}} \in \mathbb{R}^+$ are the components of the distance vector $\vec{d}_{ij}$ with respect to a global frame, $\alpha_{ij} \in \mathbb{R}$ is the formation angle measured from the distance vector $\vec{d}_{ij}$ to a local frame attached to the follower agent, as is shown in Figure 1. Once the model is obtained, the second subproblem has to be solved. A robust feedback control law has to be designed, such that:

- Leader tracks a prescribed trajectory, i.e.,

$$\lim_{t\to\infty}(\chi_n - \chi^*) = 0,$$

where $\chi^* = \begin{bmatrix}\chi_x^* & \chi_y^*\end{bmatrix}^\top \in \mathbb{R}^2$ is the desired trajectory;

- Agent R_i maintains a desired distance d_{ij}^* and a desired formation angle α_{ij}^* with respect to the agent R_j, i.e.,

$$\lim_{t\to\infty}(\boldsymbol{\eta}_{ij} - \boldsymbol{\eta}_{ij}^*) = 0,$$

where $\boldsymbol{\eta}_{ij}^* = \begin{bmatrix}d_{ij}^* & \alpha_{ij}^*\end{bmatrix}^\top$ is the vector that contains the desired distance d_{ij}^* and the desired formation angle α_{ij}^*.

It is worth pointing out that both control tasks have to be realized effectively despite the influence of perturbations such as the lateral and longitudinal slipping parameters of the wheels, sensor noises, and/or measurement errors.

3. Proposed Control System

3.1. Leader–Follower Scheme Based on Distance and Formation Angle between the Agents

Before designing the control law, the kinematic model based on distance and formation angle between the agents has to be obtained. Based on Figure 1, the distance d_{ij} and the angle α_{ij} are defined as

$$d_{ij} = \left|\vec{d}_{ij}\right| = \sqrt{d_{x_{ij}}^2 + d_{y_{ij}}^2}, \tag{3a}$$

$$\alpha_{ij} = \theta_i - \tan^{-1}\left(\frac{d_{y_{ij}}}{d_{x_{ij}}}\right), \tag{3b}$$

where $d_{x_{ij}} = \chi_{x_j} - \chi_{x_i}$ and $d_{y_{ij}} = \chi_{y_j} - \chi_{y_i}$. The time-derivative of (3) is calculated as

$$\dot{d}_{ij} = \frac{d_{x_{ij}}\dot{d}_{x_{ij}} + d_{y_{ij}}\dot{d}_{y_{ij}}}{d_{ij}}, \tag{4a}$$

$$\dot{\alpha}_{ij} = \dot{\theta}_i - \frac{d_{x_{ij}}\dot{d}_{y_{ij}} - d_{y_{ij}}\dot{d}_{x_{ij}}}{d_{ij}^2}, \tag{4b}$$

where

$$\dot{d}_{x_{ij}} = v_j\cos\theta_j - v_i\cos\theta_i - l\omega_j\sin\theta_j + l\omega_i\sin\theta_i + \varphi_{x_j} - \varphi_{x_i}, \tag{5a}$$

$$\dot{d}_{y_{ij}} = v_j\sin\theta_j - v_i\sin\theta_i + l\omega_j\cos\theta_j - l\omega_i\cos\theta_i + \varphi_{y_j} - \varphi_{y_i}. \tag{5b}$$

Substituting (5) into (4) and considering $d_{x_{ij}} = d_{ij}\cos(\theta_i - \alpha_{ij})$ and $d_{y_{ij}} = d_{ij}\sin(\theta_i - \alpha_{ij})$, the kinematics of d_{ij} and α_{ij} can be expressed as follows

$$\dot{\boldsymbol{\eta}}_{ij} = A_{ij}(\theta_i, \theta_j, \boldsymbol{\eta}_{ij})\mathbf{u}_j - B_{ij}(\boldsymbol{\eta}_{ij})\mathbf{u}_i + \boldsymbol{\varphi}_{ij}, \tag{6}$$

with

$$A_{ij} = \begin{bmatrix} \cos(\alpha_{ij} - \theta_i + \theta_j) & -l\sin(\alpha_{ij} - \theta_i + \theta_j) \\ -\frac{\sin(\alpha_{ij} - \theta_i + \theta_j)}{d_{ij}} & -\frac{l}{d_{ij}}\cos(\alpha_{ij} - \theta_i + \theta_j) \end{bmatrix},$$

$$B_{ij} = \begin{bmatrix} \cos\alpha_{ij} & -l\sin\alpha_{ij} \\ -\frac{\sin\alpha_{ij}}{d_{ij}} & -\left(1 + \frac{l}{d_{ij}}\cos\alpha_{ij}\right) \end{bmatrix},$$

$$\boldsymbol{\varphi}_{ij} = \begin{bmatrix} \cos(\theta_i - \alpha_{ij}) & \sin(\theta_i - \alpha_{ij}) \\ \frac{1}{d_{ij}}\sin(\theta_i - \alpha_{ij}) & -\frac{1}{d_{ij}}\cos(\theta_i - \alpha_{ij}) \end{bmatrix} \begin{bmatrix} \varphi_{x_j} - \varphi_{x_i} \\ \varphi_{y_j} - \varphi_{y_i} \end{bmatrix}.$$

Proposition 1. *Matrix B_{ij} is non singular for all $\cos\alpha_{ij} \neq -\frac{l}{d_{ij}}$ and $j \neq i$.*

Proof. The determinant of matrix B_{ij} is given by

$$\det(B_{ij}) = -\left(\frac{l}{d_{ij}} + \cos\alpha_{ij}\right).$$

It becomes evident that a singularity will appear when $\cos\alpha_{ij} = -\frac{l}{d_{ij}}$. Since l and $d_{ij} > 0$, the singularity can appear when

$$\alpha_{ij} \in \left(-\frac{3}{2}\pi, -\frac{\pi}{2}\right) \cup \left(\frac{\pi}{2}, \frac{3}{2}\pi\right) \tag{7}$$

With these values of α_{ij}, it means that the leader agent is outside of the field of view of the follower. On the other hand, one can select d_{ij} sufficiently larger than l to ensure the follower do not collide with his own leader. □

Let us now define the tracking error as $\mathbf{e}_{ij} = \boldsymbol{\eta}_{ij} - \boldsymbol{\eta}^*_{ij}$, with its dynamics given by

$$\dot{\mathbf{e}}_{ij} = A_{ij}(\theta_i, \theta_j, \boldsymbol{\eta}_{ij})\mathbf{u}_j - B_{ij}(\boldsymbol{\eta}_{ij})\mathbf{u}_i + \boldsymbol{\varphi}_{ij} - \dot{\boldsymbol{\eta}}^*_{ij}. \tag{8}$$

Note that (8) can be simplified to a perturbed error system

$$\dot{\mathbf{e}}_{ij} = -B_{ij}(\boldsymbol{\eta}_{ij})\mathbf{u}_i + \boldsymbol{\Phi}_{ij}(t), \tag{9}$$

where $\boldsymbol{\Phi}_{ij}(t)$ is the *total disturbance* vector (that affects the R_i agent), which has to be estimated and its influence cancelled. For the considered system, it is defined as

$$\boldsymbol{\Phi}_{ij}(t) = A_{ij}(\theta_i, \theta_j, \boldsymbol{\eta}_{ij})\mathbf{u}_j + \boldsymbol{\varphi}_{ij} - \dot{\boldsymbol{\eta}}^*_{ij}.$$

The term $\boldsymbol{\Phi}_{ij}(t)$ lumps: (i) the effects of neglected internal and external kinematics given by $A_{ij}(\theta_i, \theta_j, \boldsymbol{\eta}_{ij})$, as well as the lateral and longitudinal slipping parameters of the wheels $\boldsymbol{\varphi}_{ij}$; (ii) the unknown velocities, such as the control input $\mathbf{u}_j$, and (iii) the desired nominal velocities $\dot{\boldsymbol{\eta}}^*_{ij}$.

3.2. Followers Control Strategy

Let us now consider the kinematic model error given in (9). In order to design the control strategy for the followers, an extended state space is proposed, with $\mathbf{z}_{ij} = \boldsymbol{\Phi}_{ij}$

$$\dot{\mathbf{e}}_{ij} = - B_{ij}(\boldsymbol{\eta}_{ij})\mathbf{u}_i + \mathbf{z}_{ij}, \tag{10a}$$

$$\dot{\mathbf{z}}_{ij} = \boldsymbol{\psi}_{ij} \approx 0. \tag{10b}$$

For the above extended system, a following high-order ESO (also known as generalized proportional-integral observer, or GPIO) in the error domain is proposed to estimate the follower *total disturbance*

$$\begin{aligned} \dot{\hat{\mathbf{e}}}_{ij} &= - B_{ij}(\boldsymbol{\eta}_{ij})\mathbf{u}_i + \hat{\mathbf{z}}_{ij} + \Lambda_i(\mathbf{e}_{ij} - \hat{\mathbf{e}}_{ij}), && \text{(11a)} \\ \dot{\hat{\mathbf{z}}}_{ij} &= \Gamma_i(\mathbf{e}_{ij} - \hat{\mathbf{e}}_{ij}), && \text{(11b)} \end{aligned}$$

where $\Lambda_i = \text{diag}\{\lambda_{x_i}, \lambda_{y_i}\} \in \mathbb{R}^{2\times 2}$ and $\Gamma_i = \text{diag}\{\gamma_{x_i}, \gamma_{y_i}\} \in \mathbb{R}^{2\times 2}$ are positive diagonal matrices. Let us define the follower estimation error $\tilde{\mathbf{e}}_{ij} = \mathbf{e}_{ij} - \hat{\mathbf{e}}_{ij}$, whose time-derivative is obtained from (10) and (11) as follows

$$\ddot{\tilde{\mathbf{e}}}_{ij} + \Lambda_i \dot{\tilde{\mathbf{e}}}_{ij} + \Gamma_i \tilde{\mathbf{e}}_{ij} = \dot{\boldsymbol{\Phi}}_{ij}. \tag{12}$$

In order to tune the observer gains, the characteristic polynomials of the follower estimation error are matched with Hurwitz polynomials as

$$I_2 s^2 + \Lambda_i s + \Gamma_i = I_2 s^2 + 2\mathbf{Z}_i \mathbf{W}_i s + \mathbf{W}_i^2,$$

where I_2 is the 2×2 identity matrix while the follower observer gain matrices are chosen as

$$\Lambda_i = 2\mathbf{Z}_i \mathbf{W}_i, \quad \Gamma_i = \mathbf{W}_i^2. \tag{13}$$

The proper selection of gains (13) allows to estimate the perturbations of the model, i.e., $\hat{\boldsymbol{\Phi}}_{ij}(t) \to \boldsymbol{\Phi}_{ij}(t)$. Based on this relation, the ADRC law can be designed as

$$\mathbf{u}_i = B_{ij}^{-1}(\boldsymbol{\eta}_{ij})\left(K_i \mathbf{e}_{ij} + \hat{\boldsymbol{\Phi}}_{ij}(t)\right). \tag{14}$$

Since $\hat{\boldsymbol{\Phi}}_{ij}(t) \to \boldsymbol{\Phi}_{ij}(t)$, the closed-loop tracking error dynamics (9)–(14) yields

$$\dot{\mathbf{e}}_{ij} + K_i \mathbf{e}_{ij} = \boldsymbol{\Phi}_{ij}(t) - \hat{\boldsymbol{\Phi}}_{ij}(t). \tag{15}$$

The gain matrix K_i can be selected using a representation of (15) in frequency domain [44], where the closed-loop tracking error characteristic polynomials can be matched with some Hurwitz polynomials

$$sI_2 + K_i := sI_2 + \bar{\mathbf{W}}_i^2,$$

where $\bar{\mathbf{W}}_i = \text{diag}\{\varpi_{x_i}, \varpi_{y_i}\} \in \mathbb{R}^{2\times 2}$ is a positive diagonal matrix, which are design parameters. Therefore, the specific control gains can be calculated as

$$K_i = \bar{\mathbf{W}}_i^2. \tag{16}$$

3.3. Leader Control Strategy

It is expected that the leader agent tracks a desired trajectory $\chi^* = \begin{bmatrix} \chi_x^* & \chi_y^* \end{bmatrix}^T$ independently of the follower agents. Hence, let us define the trajectory leader error as $\mathbf{e}_{\chi_n} = \chi_n - \chi^*$, whose kinematics is given by

$$\dot{\mathbf{e}}_{\chi_n} = A_n(\theta_n, l)\mathbf{u}_n + \boldsymbol{\varphi}_n - \dot{\chi}^*. \tag{17}$$

The error dynamics (17) can be expressed as a simplified perturbed system defined as

$$\dot{\mathbf{e}}_{\chi_n} = A_n(\theta_n, l)\mathbf{u}_n + \boldsymbol{\Phi}_n, \tag{18}$$

with $\boldsymbol{\Phi}_n$ as the *total disturbance* of the leader agent

$$\boldsymbol{\Phi}_n = \boldsymbol{\varphi}_n - \dot{\chi}^*. \tag{19}$$

To design the leader control strategy, an extended state space, with $\mathbf{z}_n = \boldsymbol{\Phi}_n$, is first introduced as

$$\dot{\mathbf{e}}_{\chi_n} = A_n(\theta_n, l)\mathbf{u}_n + \mathbf{z}_n, \tag{20a}$$
$$\dot{\mathbf{z}}_n = \boldsymbol{\psi}_n \approx 0, \tag{20b}$$

for which an error-based GPIO can be designed to estimate the leader *total disturbance*, as follows

$$\dot{\hat{\mathbf{e}}}_{\chi_n} = A_n(\theta_n, l)\mathbf{u}_n + \hat{\mathbf{z}}_n + \Lambda_n(\mathbf{e}_{\chi_n} - \hat{\mathbf{e}}_{\chi_n}), \tag{21a}$$
$$\dot{\hat{\mathbf{z}}}_n = \Gamma_n(\mathbf{e}_{\chi_n} - \hat{\mathbf{e}}_{\chi_n}), \tag{21b}$$

where $\Lambda_n = \mathrm{diag}\{\lambda_{x_n}, \lambda_{y_n}\}$ and $\Gamma_n^L = \mathrm{diag}\{\gamma_{x_n}, \gamma_{y_n}\} \in \mathbb{R}^{2\times 2}$ are positive diagonal matrices. The leader estimation error is defined as $\tilde{\mathbf{e}}_n = \mathbf{e}_{\chi_n} - \hat{\mathbf{e}}_{\chi_n}$ and its dynamics are obtained from (20) and (21) as follows

$$\ddot{\tilde{\mathbf{e}}}_n + \Lambda_n\dot{\tilde{\mathbf{e}}}_n + \Gamma_n\tilde{\mathbf{e}}_n = \dot{\boldsymbol{\Phi}}_n. \tag{22}$$

In order to select the observer gains, the characteristic polynomials of leader estimation error are matched with Hurwitz polynomials

$$I_2s^2 + \Lambda_n s + \Gamma_n = I_2s^2 + 2\mathbf{Z}_n\mathbf{W}_n s + \mathbf{W}_n^2,$$

where the follower observer gain matrices are chosen as

$$\Lambda_n = 2\mathbf{Z}_n\mathbf{W}_n, \quad \Gamma_n = \mathbf{W}_n^2. \tag{23}$$

The proper selection of gains (23) allows to estimate the perturbations of the model, i.e., $\hat{\boldsymbol{\Phi}}_n(t) \to \boldsymbol{\Phi}_n(t)$. Based on this concept, the ADRC for the leader can be designed as

$$\mathbf{u}_n = -A_n^{-1}(\theta_n, l)\big(K_n\mathbf{e}_{\chi_n} + \hat{\boldsymbol{\Phi}}_n(t)\big). \tag{24}$$

Since the *total disturbance* $\boldsymbol{\Phi}_n$ can be estimated (which is valid since it can be expressed in terms of the input signal, the output signal, and the algebraic combination of their finite time derivatives), then, the closed-loop tracking error dynamics (18)–(24) yields

$$\dot{\mathbf{e}}_n + K_n\mathbf{e}_n = \boldsymbol{\Phi}_n(t) - \hat{\boldsymbol{\Phi}}_n(t). \tag{25}$$

The gain matrix K_n can be selected using a representation of (25) in frequency domain, where the closed-loop tracking leader error characteristic polynomials are matched with Hurwitz polynomials as follows

$$sI_2 + K_n := sI_2 + \bar{\mathbf{W}}_n^2, \tag{26}$$

where $\bar{\mathbf{W}}_n = \mathrm{diag}\{\varpi_{x_n}, \varpi_{y_n}\} \in \mathbb{R}^{2\times 2}$ are the design parameters. The specific control gains can be calculated as

$$K_n = \bar{\mathbf{W}}_n^2. \tag{27}$$

In the next section, the above proposed control system will be verified in a practical environment utilizing a set of laboratory mobile robots.

4. Experimental Validation

In this section, the experimental results are validated. In the first step, the experimental platform is described. Then, two experiments are performed. In the former one, a comparison between the proposed approach and a PI controller is developed, while in the second case, a platform with a slope is added, which acts as a disturbance to the robots, to verify the robustness of the proposed approach.

4.1. Experimental Platform

To perform real-time experiments, laboratory differential-drive mobile robots were constructed (see Figure 2a). They use two 12V POLOLU 37D gear motors, each with a gear ratio of 1:30, and a built-in encoder with a resolution of 64 counts per revolution. An STM32F4 Discovery board is used as a data acquisition card, and the communication between the computer and the robot is realized in real-time using a publicly available “waijung1504” MATLAB/Simulink library, Bluetooth connection, and an ESP32 microcontroller as is shown in Figure 3. The setup runs inside a controlled environment with a set of 10 infrared cameras manufactured by VICON© with a precision of 0.5 [mm] that measure the position and orientation of each robot in an area of 5×4 [m^2] with a sample time of 0.005 s. Each robot has several reflective markers with different patterns to be detectable by the TRACKER© cameras’ software (see Figure 2b).

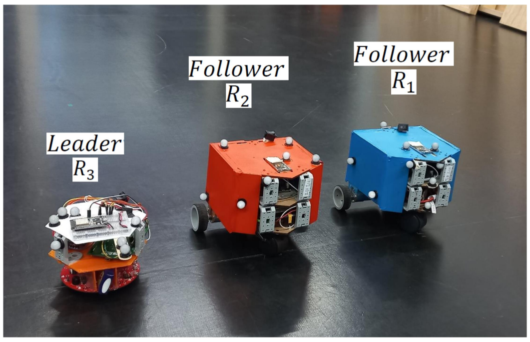

(**a**)

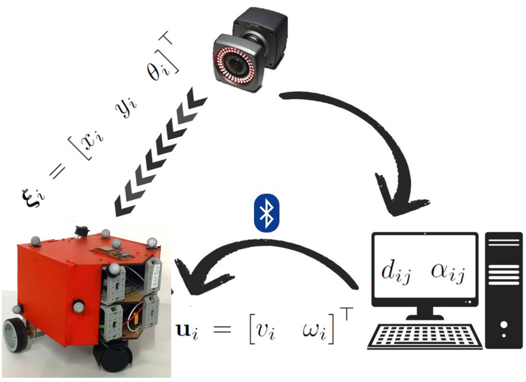

(**b**)

Figure 2. Overview of the experimental setup. (**a**) Differential-drive wheeled robots used in the test. (**b**) Communication flow chart.

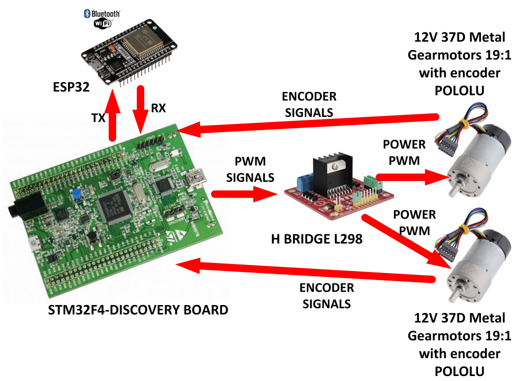

Figure 3. General scheme of the experimental platform (differential-drive robot).

Remark 3. *The communication between the computer and the differential-drive mobile robots is made through Bluetooth. In this work it is assumed that the wireless communication errors are assumed to be so small that they do not affect the performance of the robots. This may be because the GPIO estimates these errors and compensates them in the control law. The study of the errors that may occur due to wireless communication is out of scope of this work; however, it is considered for future work.*

The tested control strategies are implemented in MATLAB/Simulink. The leader observer gains (23) are set to $\mathbf{Z}_3 = \text{diag}\{7, 7\}$ and $\mathbf{W}_3 = \text{diag}\{40, 40\}$ while the control gains for the leader (27) are set to $\bar{\mathbf{W}}_3 = \text{diag}\{1.2, 1.2\}$. On the other hand, the follower observer gains (13) are set to $\mathbf{Z}_1 = \mathbf{Z}_2 = \text{diag}\{4, 4\}$ and $\mathbf{W}_1 = \mathbf{W}_2 = \{30, 30\}$, while the control gains (16) are set to $\bar{\mathbf{W}}_1 = \bar{\mathbf{W}}_2 = \text{diag}\{1.2, 1.2\}$.

To verify the robustness of the proposed GPIO approach, a Proportional-Integral (PI) control strategy is applied to the system (9) and (17). In this sense, the control strategies given in (14) and (24) are modified as follows

$$\mathbf{u}_{i_{PI}} = B_{ij}^{-1}(\boldsymbol{\eta}_{ij})\left(K_{i_{PI}}\mathbf{e}_{ij} + K_{ii_{PI}}\int_0^t \mathbf{e}_{ij}(\tau)d\tau\right),$$
$$\mathbf{u}_{n_{PI}} = -A_n^{-1}(\theta_n, l)\left(K_{n_{PI}}\mathbf{e}_{\chi_n} + K_{ni_{PI}}\int_0^t \mathbf{e}_{\chi_n}(\tau)d\tau\right),$$

for the followers and the leader, respectively. The PI gain matrices are chosen as

$$K_{i_{PI}} = 2\mathbf{W}_{i_{PI}}, \quad K_{ii_{PI}} = \mathbf{W}_{i_{PI}}^2, \quad \mathbf{W}_{i_{PI}} = \frac{\bar{\mathbf{W}}_i^2}{2}.$$
$$K_{n_{PI}} = 2\mathbf{W}_{n_{PI}}, \quad K_{ni_{PI}} = \mathbf{W}_{n_{PI}}^2, \quad \mathbf{W}_{n_{PI}} = \frac{\bar{\mathbf{W}}_i^2}{2}.$$

For a fair comparison, the gains of the GPIO and PI controllers where chosen with the same $\bar{\mathbf{W}}_i = \text{diag}\{1.2, 1.2\}$.

4.2. First Experiment

The trajectory in the plane of the three differential-drive robots is depicted in Figure 4, where the leader (blue line) is tracking a circular trajectory of radius 0.5 m, which is accomplished in 30 s, while the first follower (depicted in red line) and the second follower (depicted in green line) maintain a desired distance $d_{12}^* = d_{23}^* = 0.25$ [m] and a desired formation angle $\alpha_{12}^* = \alpha_{23}^* = \frac{\pi}{2}$ [rad] for $t = [0, 15]$ [s] and $\alpha_{12}^* = \alpha_{23}^* = \frac{\pi}{4}$ [rad] for $t = [15, 30]$ [s]. Specifically, Figure 4a shows the trajectory in the plane with the GPIO approach while Figure 4b shows the trajectory in the plane with a PI controller.

Figure 5a illustrates a comparison between the GPIO and the PI of the leader's trajectory while Figure 5b shows the leader's position error. Such errors are oscillating around zero (± 0.001 m in steady-sate) therefore, the leader reaches its desired trajectory. It becomes evident that the performance of both control strategies is quite similar.

The distance and formation angle among the mobile robots is shown in Figure 6. It can be noticed that when using the GPIO approach, the agents converge to the desired distance between them, i.e., $d_{12} \approx d_{12}^*$ and $d_{23} \approx d_{23}^*$. In the same way, the formation angles converge to the desired angle, i.e., $\alpha_{12} \approx \alpha_{12}^*$ and $\alpha_{23} \approx \alpha_{23}^*$ with $\alpha_{12}^* = \alpha_{23}^* = \frac{\pi}{2}$ [rad] for $0 \leq t < 15$ [s]. Furthermore, when the desired formation angle changes to $\alpha_{12}^* = \alpha_{23}^* = \frac{\pi}{4}$ [rad] for $15 \leq t \leq 30$ [s], the control is able to keep the distances between the agents. On the other hand, when using the PI controller, oscillations of greater amplitude are presented. This behavior is also seen in Figure 7, where the distance and formation angle errors are displayed. One can note that the errors are closer to zero with the GPIO approach.

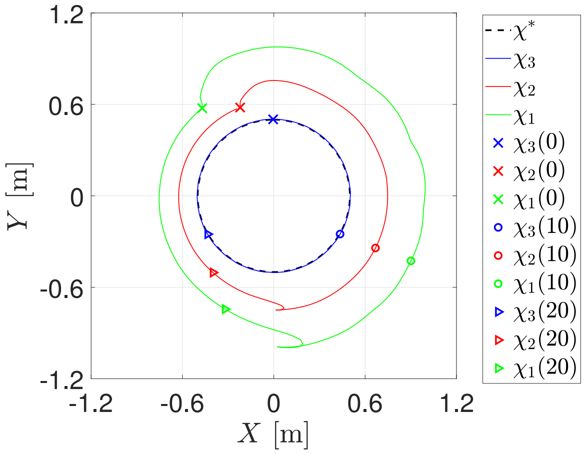

(**a**)

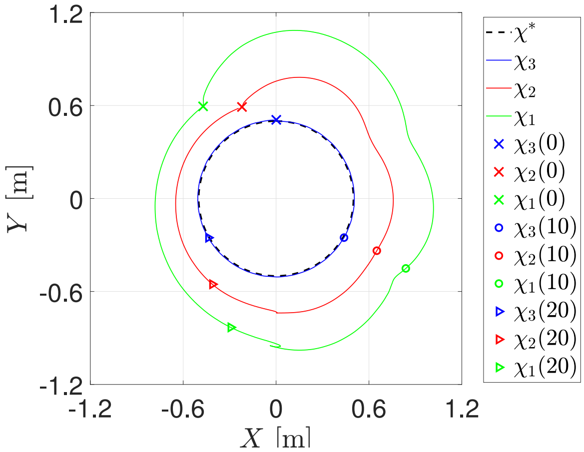

(**b**)

Figure 4. Trajectory in the plane of the mobile robots for the first experiment. (**a**) Trajectory in the plane with the GPIO approach. (**b**) Trajectory in the plane with the PI approach.

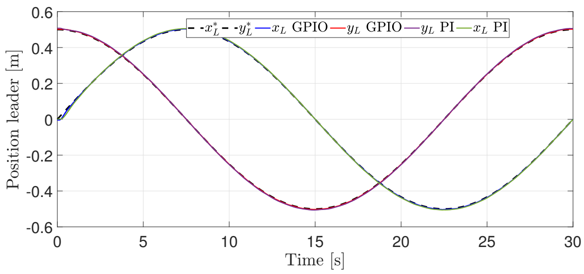

(**a**)

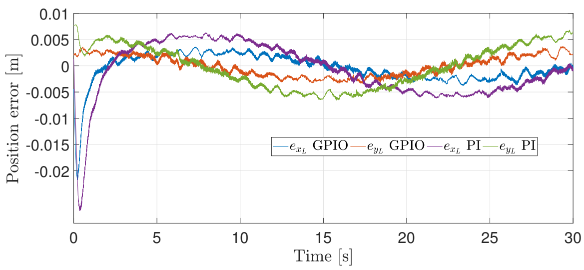

(**b**)

Figure 5. Leader trajectory tracking performance. (**a**) Leader tracking for the first experiment. (**b**) Leader trajectory error.

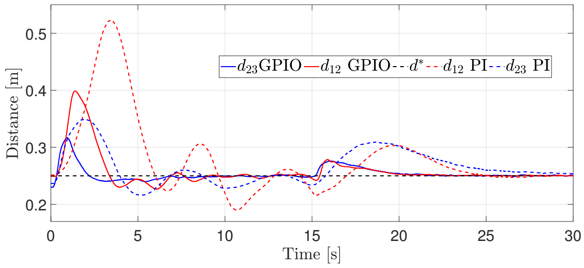

(**a**)

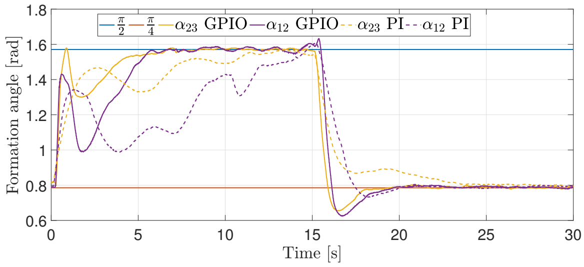

(**b**)

Figure 6. Distances and formation angles between the robots for the first experiment. (**a**) Distances between the robots. (**b**) Formation angles between the robots.

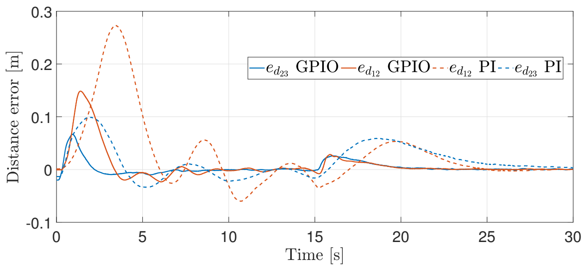

(**a**)

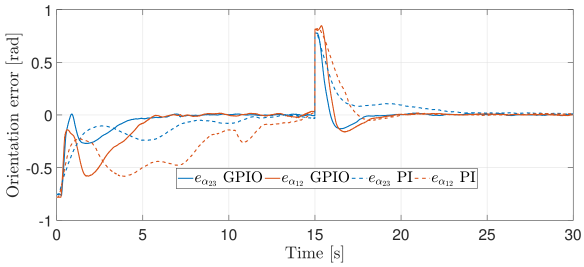

(**b**)

Figure 7. Distances and orientation angles errors for the first experiment. (**a**) Distance error. (**b**) Orientation error.

A comparison, between the control inputs, given by the GPIO approach and the PI controller, is given in Figure 8. One can note oscillations of greater amplitude with the PI controller.

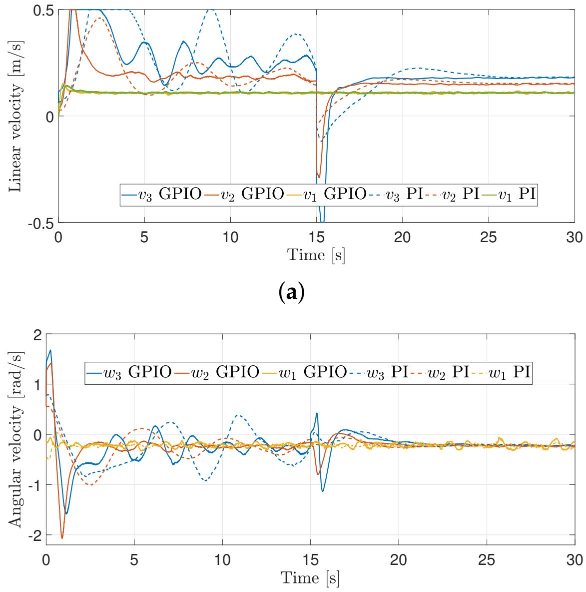

(**a**)

(**b**)

Figure 8. Control inputs for the robots for the first experiment. (**a**) Longitudinal velocities. (**b**) Angular velocities.

4.3. Second Experiment

For the second experiment, we used an uneven surface with 10 degrees of slope that is collocated such that it acts as a disturbance to the agents (see Figure 9). Furthermore, the parameters are the same as in the previous experiment.

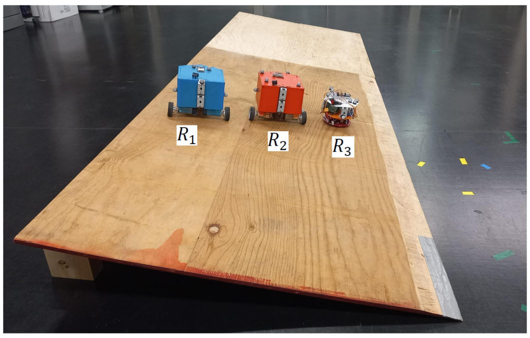

Figure 9. Uneven surface as a disturbance experimental test.

The trajectory in the three-dimensional space of the three differential-drive robots is depicted in Figure 10, while the trajectory in the plane is shown in Figure 11. Specifically, Figure 11a shows the trajectory in the plane with the GPIO approach, while Figure 11b shows the trajectory in the plane with a PI controller.

Figure 12a illustrates a comparison between the GPIO and the PI of the leader's trajectory, while Figure 12b shows the leader's position error. Note that when the leader enters the uneven surface, the position error increases. However, the GPIO approach can deal with these perturbations, while with the PI controller, the position error has oscillations of greater amplitude.

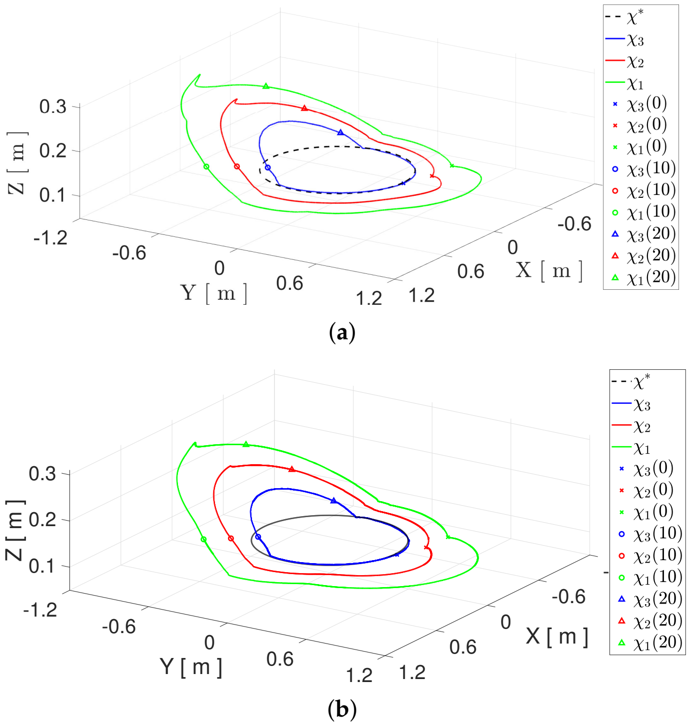

Figure 10. Trajectory in the three dimensional space of the mobile robots for the second experiment. (**a**) Trajectory in the three dimensional space with the GPIO approach. (**b**) Trajectory in the three dimensional space with the PI approach.

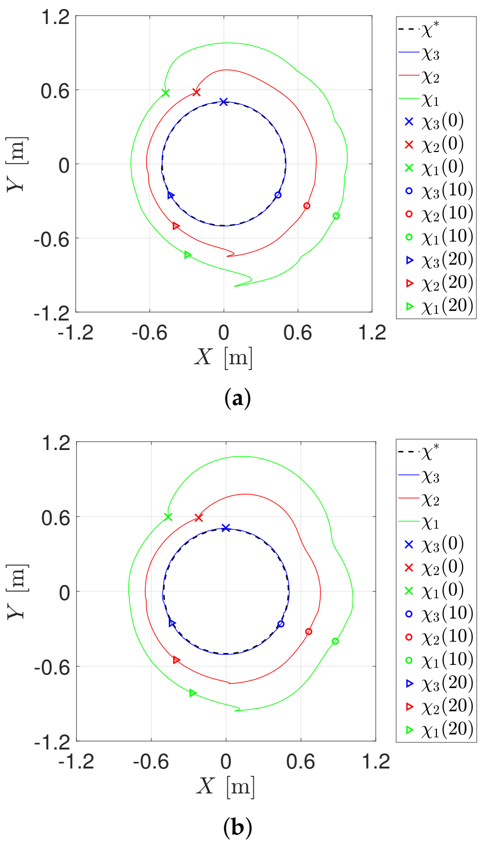

Figure 11. Trajectory in the plane of the mobile robots for the second experiment. (**a**) Trajectory in the plane with the GPIO approach. (**b**) Trajectory in the plane with the PI approach.

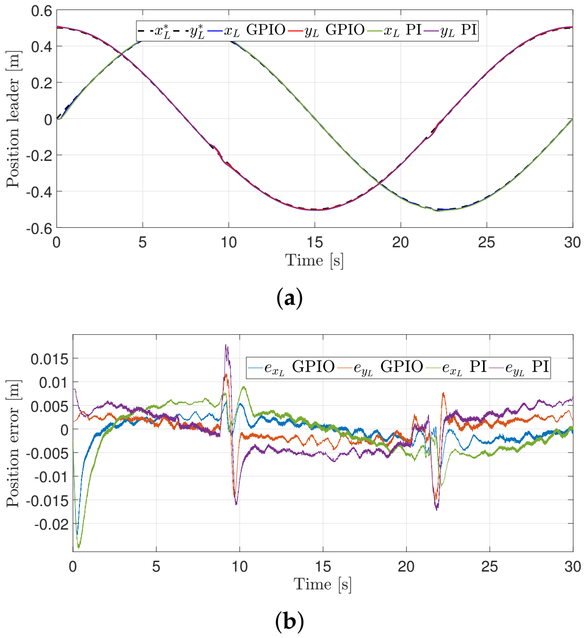

Figure 12. Leader trajectory tracking performance for the second experiment. (**a**) Leader tracking. (**b**) Leader trajectory error.

The distance and formation angle among the mobile robots is shown in Figure 13. It can be noticed that when using the GPIO approach, the agents converge to the desired distance and formation angle, even in the presence of the uneven surface. Otherwise, with the PI controller, which is not capable of dealing with the disturbance, in addition to presenting oscillations of greater amplitude. This behavior is also seen in Figure 14, where the distance and formation angle errors are displayed.

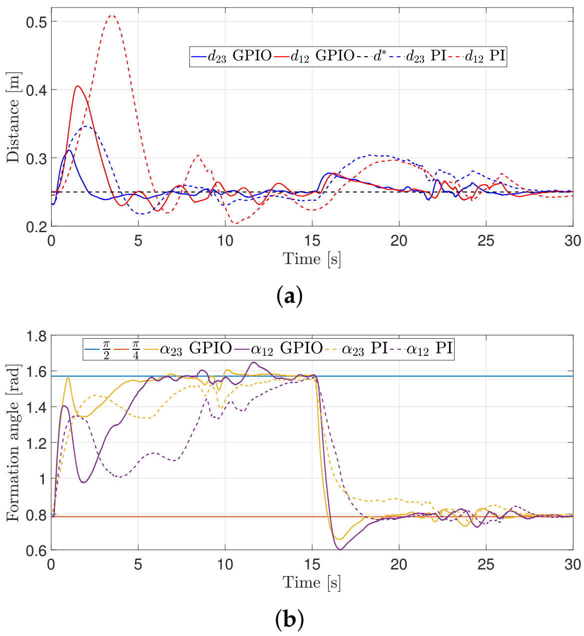

Figure 13. Distances and formation angles between the robots for the second experiment. (**a**) Distances between the robots. (**b**) Formation angles between the robots.

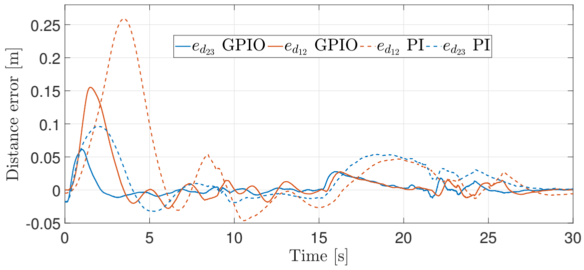

(**a**)

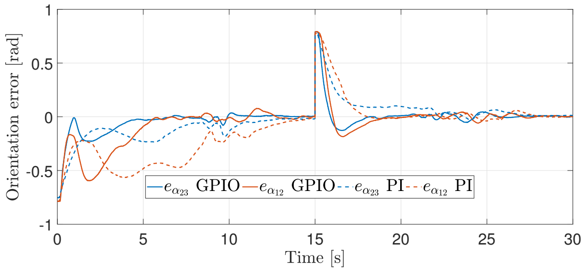

(**b**)

Figure 14. Distances and orientation angles errors for the second experiment. (**a**) Distance error. (**b**) Orientation error.

A comparison between the control inputs, given by the GPIO approach and the PI controller, is given in Figure 15.

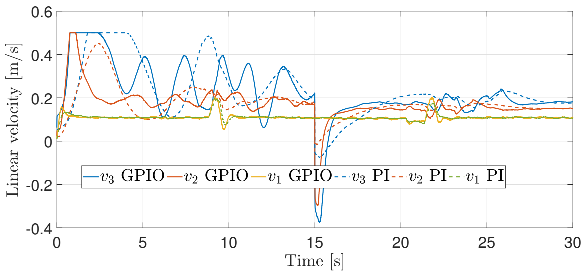

(**a**)

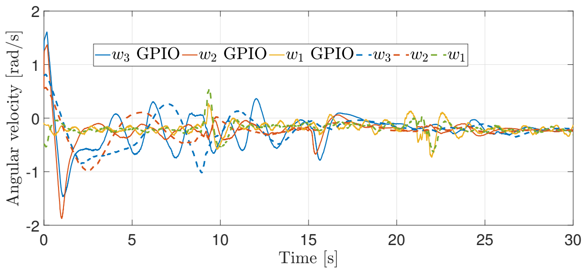

(**b**)

Figure 15. Control inputs for the robots for the second experiment. (**a**) Longitudinal velocities. (**b**) Angular velocities.

Finally, Figure 16 presents the disturbance estimation of each agent, which was used for the disturbance cancellation effects.

Remark 4. *It is worth mentioning that similar results will be obtained despite having different initial conditions regarding the distance between agents. However, the restriction given in* (7) *must be considered. This implies that the leader agent must be in line of sight of the follower agent. Furthermore, the initial distances of the robots are defined from their initial positions according to Equation* (3a).

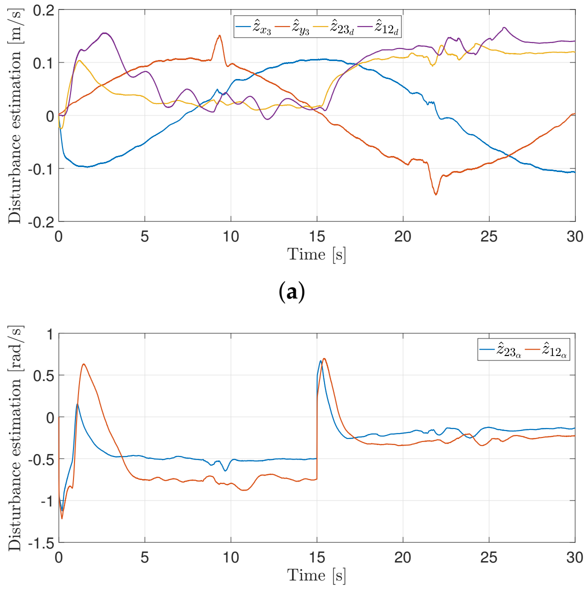

(**a**)

(**b**)

Figure 16. On line total disturbance estimation. (**a**) Total disturbance estimation of the longitudinal velocity. (**b**) Total disturbance estimation of angular velocity.

A real time experiment of the performance of the differential-drive robots can be watched on the link in Supplementary Material.

5. Conclusions

In this work, the problem of designing an ADRC for differential-drive mobile robots operating in a leader–follower configuration is solved by firstly developing a kinematic model based on distance and formation angle between agents. A specific case of trajectory tracking is considered without the use of signal time-derivatives in the controller. The utilized control task reformulation to error-domain allowed the unmeasured time-derivatives to be conveniently reconstructed with a custom observer, which benefits the practical appeal of the proposed control scheme.

Mobile robots are usually exposed to time delays in communication. This can be overcome by predictor-based schemes (e.g., [22]) or making the delay as part of the control design (e.g., [45,46]). The ADRC could be thus combined in the future with such methods to increase their performance.

Supplementary Materials: Some evidence of the experimental results is provided in the following video: https://www.youtube.com/watch?v=J0qHcUQ-17o (accessed on 17 October 2022).

Author Contributions: Conceptualization, M.R.-N. and J.G.-S.; methodology, R.M., N.L.-C. and A.L.-J.; software, M.R.-N. and R.M.; validation, M.R.-N., J.G.-S. and R.M.; formal analysis, J.G.-S., R.M., N.L.-C. and A.L.-J.; investigation, M.R.-N., J.G.-S., R.M., N.L.-C. and A.L.-J.; resources, M.R.-N., J.G.-S., R.M., N.L.-C. and A.L.-J.; data curation, M.R.-N., J.G.-S. and R.M.; writing—original draft preparation, M.R.-N., J.G.-S., R.M., N.L.-C. and A.L.-J.; writing—review and editing, M.R.-N., J.G.-S., R.M., N.L.-C. and A.L.-J.; visualization, M.R.-N., J.G.-S., R.M., N.L.-C. and A.L.-J.; supervision, M.R.-N., R.M. and A.L.-J.; project administration, M.R.-N., J.G.-S., R.M., N.L.-C. and A.L.-J.; funding acquisition, M.R.-N. and A.L.-J. All authors have read and agreed to the published version of the manuscript.

Funding: This research was funded by Secretaría de Investigación y Posgrado SIP IPN under grants 20220623, 20220633, and by the Universidad Iberoamericana Ciudad de México, División de Investigación y Posgrado (DINVP), Ciudad de México, México, under Grant 25.

Data Availability Statement: Not applicable.

Conflicts of Interest: The authors declare no conflict of interest.

Abbreviations

The following abbreviations are used in this manuscript:

ADRC	Active Disturbance Rejection Control
PID	Proportional Integral Derivative Control
ESO	Extended State Observer
GPIO	Generalized Proportional Integral Observer

References

1. Yan, Z.; Jouandeau, N.; Cherif, A.A. A survey and analysis of multi-robot coordination. *Int. J. Adv. Robot. Syst.* **2013**, *10*, 399. [CrossRef]
2. Feng, Z.; Hu, G.; Sun, Y.; Soon, J. An overview of collaborative robotic manipulation in multi-robot systems. *Annu. Rev. Control* **2020**, *49*, 113–127. [CrossRef]
3. Ren, W.; Beard, R.W. *Distributed Consensus in Multi-Vehicle Cooperative Control*; Springer: Berlin/Heidelberg, Germany, 2008.
4. Wang, X.; Li, S.; Yu, X.; Yang, J. Distributed active anti-disturbance consensus for leader-follower higher-order multi-agent systems with mismatched disturbances. *IEEE Trans. Autom. Control* **2016**, *62*, 5795–5801. [CrossRef]
5. González-Sierra, J.; Hernández-Martínez, E.G.; Ferreira-Vazquez, E.D.; Flores-Godoy, J.J.; Fernandez-Anaya, G.; Paniagua-Contro, P. Leader-follower control strategy with rigid body behavior. *IFAC-PapersOnLine* **2018**, *51*, 184–189. [CrossRef]
6. Wang, X.; Liu, W.; Wu, Q.; Li, S. A Modular Optimal Formation Control Scheme of Multiagent Systems With Application to Multiple Mobile Robots. *IEEE Trans. Ind. Electron.* **2022**, *69*, 9331–9341. [CrossRef]
7. Hernández-Martínez, E.G.; Aranda-Bricaire, E. Trajectory tracking for groups of unicycles with convergence of the orientation angles. In Proceedings of the IEEE Conference on Decision and Control, Atlanta, GA, USA, 15–17 December 2010; pp. 6323–6328.
8. Desai, J.P.; Ostrowski, J.P.; Kumar, V. Modeling and control of formations of nonholonomic mobile robots. *IEEE Trans. Robot. Autom.* **2001**, *17*, 905–908. [CrossRef]
9. Deghat, M.; Shames, I.; Anderson, B.D.O.; Yu, C. Localization and Circumnavigation of a Slowly Moving Target Using Bearing Measurements. *IEEE Trans. Autom. Control* **2014**, *59*, 2182–2188. [CrossRef]
10. Shames, I.; Dasgupta, S.; Fidan, B.; Anderson, B.D.O. Circumnavigation Using Distance Measurements Under Slow Drift. *IEEE Trans. Autom. Control* **2012**, *57*, 889–903. [CrossRef]
11. Shao, J.; Tian, Y.P. Multi-target localization and circumnavigation control by a group of moving agents. In Proceedings of the IEEE International Conference on Control Automation, Ohrid, Macedonia, 3–6 July 2017; pp. 606–611.
12. Boccia, A.; Adaldo, A.; Dimarogonas, D.V.; di Bernardo, M.; Johansson, K.H. Tracking a mobile target by multi-robot circumnavigation using bearing measurements. In Proceedings of the IEEE Conference on Decision and Control, Melbourne, Australia, 12–15 December 2017; pp. 1076–1081.
13. Zhong, H.; Miao, Y.; Tan, Z.; Li, J.; Zhang, H.; Fierro, R. Circumnavigation of a Moving Target in 3D by Multi-agent Systems with Collision Avoidance: An Orthogonal Vector Fields-based Approach. *Int. J. Control Autom. Syst.* **2019**, *17*, 212–224. [CrossRef]
14. Shen, D.; Sun, Z.; Sun, W. Leader-follower formation control without leader's velocity information. *Sci. China Inf. Sci.* **2014**, *57*, 1–12. [CrossRef]
15. Zhao, Y.; Zhang, Y.; Lee, J. Lyapunov and Sliding Mode Based Leader-follower Formation Control for Multiple Mobile Robots with an Augmented Distance-angle Strategy. *Int. J. Control Autom. Syst.* **2019**, *17*, 1314–1321. [CrossRef]
16. Hua, C.C.; Liu, X.P. Delay-Dependent Stability Criteria of Teleoperation Systems with Asymmetric Time-Varying Delays. *IEEE Trans. Robot.* **2010**, *26*, 925–932. [CrossRef]
17. Saha, O.; Dasgupta, P. A comprehensive survey of recent trends in cloud robotics architectures and applications. *Robotics* **2018**, *7*, 47. [CrossRef]
18. Toris, R.; Kammerl, J.; Lu, D.V.; Lee, J.; Jenkins, O.C.; Osentoski, S.; Wills, M.; Chernova, S. Robot web tools: Efficient messaging for cloud robotics. In Proceedings of the IEEE/RSJ International Conference on Intelligent Robots and Systems (IROS), Hamburg, Germany, 28 September–3 October 2015; pp. 4530–4537.
19. Diddeniya, I.; Wanniarachchi, I.; Gunasinghe, H.; Premachandra, C.; Kawanaka, H. Human–Robot Communication System for an Isolated Environment. *IEEE Access* **2022**, *10*, 63258–63269. [CrossRef]
20. Panchi, F.; Hernández, K.; Chávez, D. MQTT Protocol of IoT for Real Time Bilateral Teleoperation Applied to Car-Like Mobile Robot. In Proceedings of the 2018 IEEE Third Ecuador Technical Chapters Meeting (ETCM), Cuenca, Ecuador, 15–19 October 2018; pp. 1–6.
21. Han, J. From PID to active disturbance rejection control. *IEEE Trans. Ind. Electron.* **2009**, *56*, 900–906. [CrossRef]
22. Sira-Ramírez, H.; Luviano-Juárez, A.; Ramírez-Neria, M.; Zurita-Bustamante, E.W. *Active Disturbance Rejection Control of Dynamic Systems: A Flatness Based Approach*; Butterworth-Heinemann: Oxford, UK, 2018.
23. Herbst, G. Practical Active Disturbance Rejection Control: Bumpless Transfer, Rate Limitation, and Incremental Algorithm. *IEEE Trans. Ind. Electron.* **2016**, *63*, 1754–1762. [CrossRef]
24. Madonski, R.; Shao, S.; Zhang, H.; Gao, Z.; Yang, J.; Li, S. General error-based active disturbance rejection control for swift industrial implementations. *Control Eng. Pract.* **2019**, *84*, 218–229. [CrossRef]

25. Gao, Z.; Zheng, Q. Active disturbance rejection control: Some recent experimental and industrial case studies. *Control Theory Technol.* **2018**, *16*, 301–313.
26. Madonski, R.; Herman, P. Survey on methods of increasing the efficiency of extended state disturbance observers. *ISA Trans.* **2015**, *56*, 18–27. [CrossRef]
27. Wu, Z.H.; Zhou, H.C.; Guo, B.Z.; Deng, F. Review and new theoretical perspectives on active disturbance rejection control for uncertain finite-dimensional and infinite-dimensional systems. *Nonlinear Dyn.* **2020**, *101*, 935–959. [CrossRef]
28. Zhang, X.; Zhang, X.; Xue, W.; Xin, B. An overview on recent progress of extended state observers for uncertain systems: Methods, theory, and applications. *Adv. Control Appl.* **2021**, *3*, e89. [CrossRef]
29. Sira-Ramírez, H.; López-Uribe, C.; Velasco-Villa, M. Linear Observer-Based Active Disturbance Rejection Control of the Omnidirectional Mobile Robot. *Asian J. Control* **2013**, *15*, 51–63. [CrossRef]
30. Ren, C.; Liu, R.; Ma, S.; Hu, C.; Cao, L. ESO Based Model Predictive Control of an Omnidirectional Mobile Robot with Friction Compensation. In Proceedings of the Chinese Control Conference, Wuhan, China, 25–27 July 2018; pp. 3943–3948.
31. Ren, C.; Zhang, M.; Ma, S.; Wei, D. Trajectory Tracking Control of an Omnidirectional Mobile Manipulator Based on Active Disturbance Rejection Control. In Proceedings of the World Congress on Intelligent Control and Automation, Changsha, China, 4–8 July 2018; pp. 1537–1542.
32. Fliess, M.; Lévine, J.; Martin, P.; Rouchon, P. Flatness and defect of non-linear systems: Introductory theory and examples. *Int. J. Control* **1995**, *61*, 1327–1361. [CrossRef]
33. Michalek, M.M. Robust trajectory following without availability of the reference time-derivatives in the control scheme with active disturbance rejection. In Proceedings of the American Control Conference, Boston, MA, USA, 6–8 July 2016; pp. 1536–1541.
34. Ramirez-Neria, M.; Madonski, R.; Shao, S.; Gao, Z. Robust tracking in underactuated systems using flatness-based ADRC with cascade observers. *J. Dyn. Syst. Meas. Control* **2020**, *142*, 091002. [CrossRef]
35. Stankovic, M.; Madonski, R.; Manojlovic, S.; Lechekhab, T.E.; Mikluc, D. Error-Based Active Disturbance Rejection Altitude/Attitude Control of a Quadrotor UAV. In *Advanced, Contemporary Control*; Springer: Berlin/Heidelberg, Germany, 2020; pp. 1348–1358.
36. Chen, S.; Chen, Z.; Zhao, Z. An error-based active disturbance rejection control with memory structure. *Meas. Control* **2021**, *54*, 724–736. [CrossRef]
37. Ramírez-Neria, M.; Madonski, R.; Luviano-Juárez, A.; Gao, Z.; Sira-Ramírez, H. Design of ADRC for Second-Order Mechanical Systems without Time-Derivatives in the Tracking Controller. In Proceedings of the American Control Conference, Denver, CO, USA, 1–3 July 2020; pp. 2623–2628.
38. Cui, M.; Huang, R.; Liu, H.; Liu, X.; Sun, D. Adaptive tracking control of wheeled mobile robots with unknown longitudinal and lateral slipping parameters. *Nonlinear Dyn.* **2014**, *2014*, 1811–1826. [CrossRef]
39. Wang, D.; Low, C.B. Modeling and Analysis of Skidding and Slipping in Wheeled Mobile Robots: Control Design Perspective. *IEEE Trans. Robot.* **2008**, *24*, 676–687. [CrossRef]
40. Li, Z.; Canny, J. *Nonholonomic Motion Planning*; Springer Science & Business Media: Berlin/Heidelberg, Germany, 1993.
41. Spong, M.W.; Hutchinson, S.; Vidyasagar, M. *Robot Modeling and Control*; John Wiley & Sons: Hoboken, NJ, USA, 2020.
42. Fareh, R.; Khadraoui, S.; Abdallah, M.Y.; Baziyad, M.; Bettayeb, M. Active disturbance rejection control for robotic systems: A review. *Mechatronics* **2021**, *80*, 102671. [CrossRef]
43. Rouchon, P.; Fliess, M.; Lévine, J.; Martin, P. Flatness and motion planning: The car with n trailers. In Proceedings of the ECC'93, Groningen, The Netherlands, 28 June–1 July 1993; pp. 1518–1522.
44. Gao, Z. Scaling and bandwidth-parameterization based controller tuning. In Proceedings of the American Control Conference, Denver, CO, USA, 4–6 June 2003; Volume 6, pp. 4989–4996.
45. Ochoa-Ortega, G.; Villafuerte-Segura, R.; Luviano-Juárez, A.; Ramírez-Neria, M.; Lozada-Castillo, N. Cascade Delayed Controller Design for a Class of Underactuated Systems. *Complexity* **2020**, *2020*, 2160743. [CrossRef]
46. Villafuerte, R.; Mondié, S.; Garrido, R. Tuning of proportional retarded controllers: Theory and experiments. *IEEE Trans. Control Syst. Technol.* **2012**, *21*, 983–990. [CrossRef]